*International Journal of Spine Surgery*, Vol. 20, No. 2, 2026, pp. 232–242
https://doi.org/10.14444/8859


# Can the Stand-Alone Cervical Interfacet Fusion Achieve Spinal Stability? A Comprehensive Finite Element Analysis

LUCA CIRIELLO, PHD[1*]; MARGHERITA ROTONDI, MSC[1*]; GIUSEPPE J. SCIARRONE, MD[2]; AND TOMASO VILLA, PHD[1]

[1]*Department of Chemistry, Materials and Chemical Engineering "Giulio Natta" - LaBS, Politecnico di Milano, Milan, Italy;* [2]*Minimally Invasive Spine Surgery, Humanitas-San Pio X Hospital, Milan, Italy*

[*]Luca Ciriello and Margherita Rotondi contributed equally to the work.

## ABSTRACT

**Background:** Degenerative pathologies of the cervical spine often involve facet and disc degeneration, leading to biomechanical instability of the cervical spine. A promising surgical solution is a cervical interfacet fusion system (CIFS), typically combined with an anterior disc cage to promote bone fusion and restore stability. However, the necessity of the anterior disc cage remains controversial because it increases surgical time, cost, and risk. The aim of this study was to evaluate the biomechanical performance of CIFS alone compared with its combination with an anterior disc cage using a C2–C7 finite element model.

**Methods:** The model was validated against literature data in terms of range of motion (RoM) and used to simulate 3 surgical scenarios: (i) anterior disc cage alone, (ii) CIFS alone, and (iii) CIFS combined with an anterior disc cage. Simulations were performed with C4–C5, C5–C6, and C4–C6 treated levels under flexion, extension, axial rotation, and lateral bending.

**Results:** Models (i) and (iii) eliminated motion at the treated levels but induced hypermobility and increased intradiscal pressure (IDP) at adjacent levels. Conversely, model (ii) preserved residual motion at the treated levels, providing mobility with RoM values within the average range of a healthy population and reducing intradiscal pressure at both the treated and adjacent levels, potentially protecting adjacent discs. However, model (ii) has a higher risk of pseudarthrosis due to the residual motion.

**Clinical Relevance:** This study highlights how a CIFS in cervical spine surgery is a cost-effective alternative that preserves mobility but requires careful patient selection to minimize risks such as pseudarthrosis and adjacent segment degeneration while emphasizing the need for postoperative muscle rehabilitation.

**Conclusions:** These results suggest that CIFS alone may provide a treatment that is both cost-effective and capable of preserving mobility with RoM values within the average range of a healthy population, especially with appropriate patient selection and muscle rehabilitation.

**Level of Evidence:** 5.

Biomechanics

Keywords: finite element model, cervical column, cervical interfacet fusion systems, anterior disc cage, cervical radiculopathy, cervical instability

## INTRODUCTION

The cervical region is considered the most complex and delicate section of the vertebral column because it protects vital structures such as the first portion of the spinal cord and blood vessels; an injury at this level is common and can result in long-term disability or even death.[1] Such injuries could be caused by trauma, leading to dislocations or fractures, or by degenerative diseases that develop slowly, mainly affecting cartilaginous structures such as the intervertebral discs and facets.[2,3] Once this chronic condition progresses, conservative treatments are ineffective, and surgery is required in terms of decompression of the nervous structures and anterior/posterior fixation with implantable devices.[4] To assess the effectiveness of these fixation systems and understand how the cervical spine may comply after their implantation, both experimental and numerical studies can be carried out.[5,6] In the past 20 years, the development of finite element models (FEMs) of the cervical spine has increased exponentially; however, they are mainly focused on posterior fixation with rods and screws, anterior fixation with cage and plate, implantation of artificial disc, or their combination. A valuable alternative to these devices is represented by cervical interfacet fusion systems (CIFSs), which allow the treatment of facet and disc degeneration by simultaneously decompressing

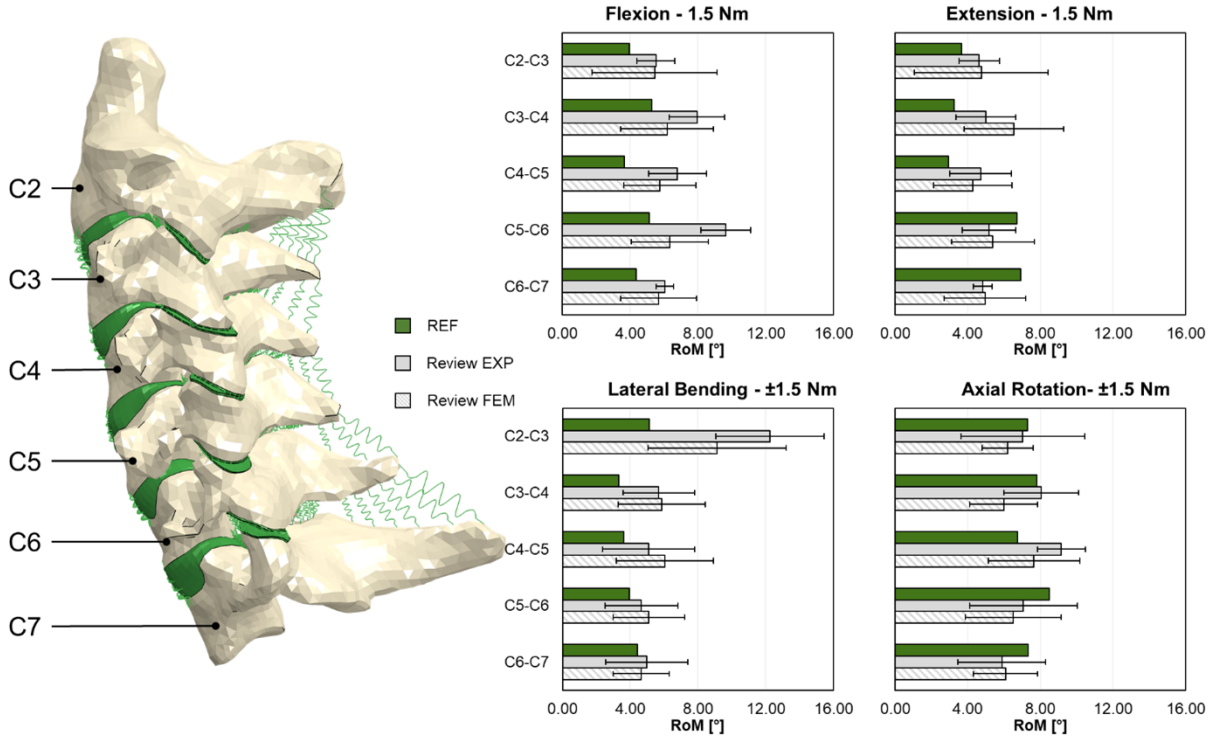


**Figure 1.** On the left, the numerical C2–C7 model is shown, while on the right, histograms of ranges of motions (RoMs) in flexion, extension, lateral bending, and axial rotation comparing the numerical model developed (REF) and reviewed experimental (review EXP) and numerical (review FEM) data are shown. EXP, experimental; FEM, finite element model; REF, reference.

the nerve roots, distracting the facet joints, and promoting fusion at the surgical level.[6] However, few studies[7–11] have analyzed the effects of these devices on the biomechanics of the cervical spine. Therefore, the present study aims to develop and validate a C2–C7 cervical FEM and use it to answer a clinical question.

In particular, in clinical practice, CIFSs are usually combined with an anterior disc cage (ADC), which leads to increased surgical time, risks, and costs associated with the surgery. Therefore, the goal of the present study is to determine whether the additional ADC is necessary or whether a stand-alone implantation of a CIFS is sufficient to achieve effective stabilization of the cervical spine.

## METHODS

### Development and Validation of the C2–C7 Model

A C2–C7 FEM was developed (Figure 1) using Abaqus (SIMULIA Inc., Providence, RI, USA) software, and was built based on the FEM developed by Herron et al.[12] Five intervertebral discs (from C1 to C5), articular facets, and ligaments (anterior longitudinal ligament, posterior longitudinal ligament, interspinous ligament, ligamentum flavum, and capsular ligament) were included.[12]

The vertebrae, disc, and facet components were modeled as continuum solid material, while the ligaments were modeled as nonlinear tension-only springs.

The material properties of the components are reported in Table 1. The mechanical properties of the ligamentous structures are assigned as nonlinear force-displacement curves.[13,14]

The element types used for the discretization were linear tetrahedrons for cortical and trabecular bone and linear hexahedrons for the other components (Table 1). Interactions between facets are modeled as general contact with normal hard behavior and frictionless as tangential behavior, while to the endplate-vertebra and the facet-vertebra interfaces, a tie constraint is assigned.[12,13]

Static analysis was conducted in 2 steps. In the first step, each intervertebral disc is axially compressed by a follower load of 50 N,[14] which simulates head weight and muscle forces. In the second step, a pure moment of ±1.5 Nm is applied on the superior vertebra and posterior facet surfaces in the sagittal, coronal, and transverse planes to simulate flexion-extension, lateral bending, and axial rotation, respectively. An encastre on the C7 inferior surface was imposed.

Parameters have been set as a result of 2 sensitivity analyses about the influence of preload's magnitude (from

**Table 1.** Material properties and mesh details for each component of the model.

| Component | Reference | Constitutive Model | Material Properties | | | | | Element Type | # Element |
|---|---|---|---|---|---|---|---|---|---|
| Disc | | | | | | | | | |
| Annulus | Lin et al[15] | Hyperelastic Holzapfel | C10 = 0.84 | D = 0.3 | k1 = 3 | k2 = 90 | k = 0.33 | C3D8 | 3900 |
| Nucleus | Lin et al[15] | Hyperelastic Mooney-Rivlin | C10 = 0.64 | C01 = 0.09 | D1 = 0.022 | | | C3D8 | 3000 |
| Endplates | Silva et al[16] | Elastic Isotropic | E = 5 MPa | ν = 0.49 | | | | C3D8 | 4600 |
| Vertebral bone | | | | | | | | | |
| Cortical | Herron et al[12] | Elastic Orthotropic | $E_1$ = 8000 MPa<br>$\nu_{23}$ = 0.35 | $E_2$ = 8000 MPa<br>$G_{12}$ = 241.4 MPa | $E_3$ = 12000 MPa<br>$G_{13}$ = 241.4 MPa | $\nu_{12}$ = 0.4<br>$G_{23}$ = 241.4 MPa | $\nu_{13}$ = 0.3 | C3D4 | 99,316 |
| Trabecular | Herron et al[12] | Hyperelastic Neo Hooke | C10 = 19.23 | D1 = 0.024 | | | | C3D4 | 99,504 |
| Facet | Herron et al[12] | Hyperelastic Neo Hooke | C10 = 1.923 | D1 = 0.24 | | | | C3D8 | 8914 |

*Note:* C10, D1, D, C01, k1, k2, and k are constitutive model constants; $E_1$, $E_2$, $E_3$, and E are elastic moduli; $G_{12}$, $G_{13}$, and $G_{23}$ are components of the shear modulus; and ν, $\nu_{12}$, $\nu_{23}$, and $\nu_{13}$ are Poisson's modulus components.

0 N to 100 N)[17] and friction (frictionless or penalty $f$ = 0.1)[18] to develop physiological modeling of the spine.

The model was validated by comparing the range of motion (RoM) of each level in terms of angle in flexion-extension, lateral bending, and axial rotation with those of a literature review of both numerical and experimental studies.[12,19–35]

## Simulation of Different Clinical Scenarios

The validated model has been employed to analyze a specific clinical study. In particular, as reported in Figure 2, x-ray images of a 60-year-old woman with 2 ADCs and 2 CIFSs implanted in C4–C5 and C5–C6 levels were provided by the Humanitas San Pio X Hospital (Milan, Italy). The patient was suffering from an intractable right cervical radiculopathy, which was caused by an osteophytic discopathy with foraminal stenosis at C4-C5-C6. Specifically, the CIFS implanted was a Sharkage (SKC) fusion system manufactured by 2B1 srl (Milan, Italy).

To evaluate the influence of the ADC, the SKC, and their combined effect, 3 different simulations were defined:

- ADC model: insertion of the ADC between the vertebral bodies, replacing the disc.

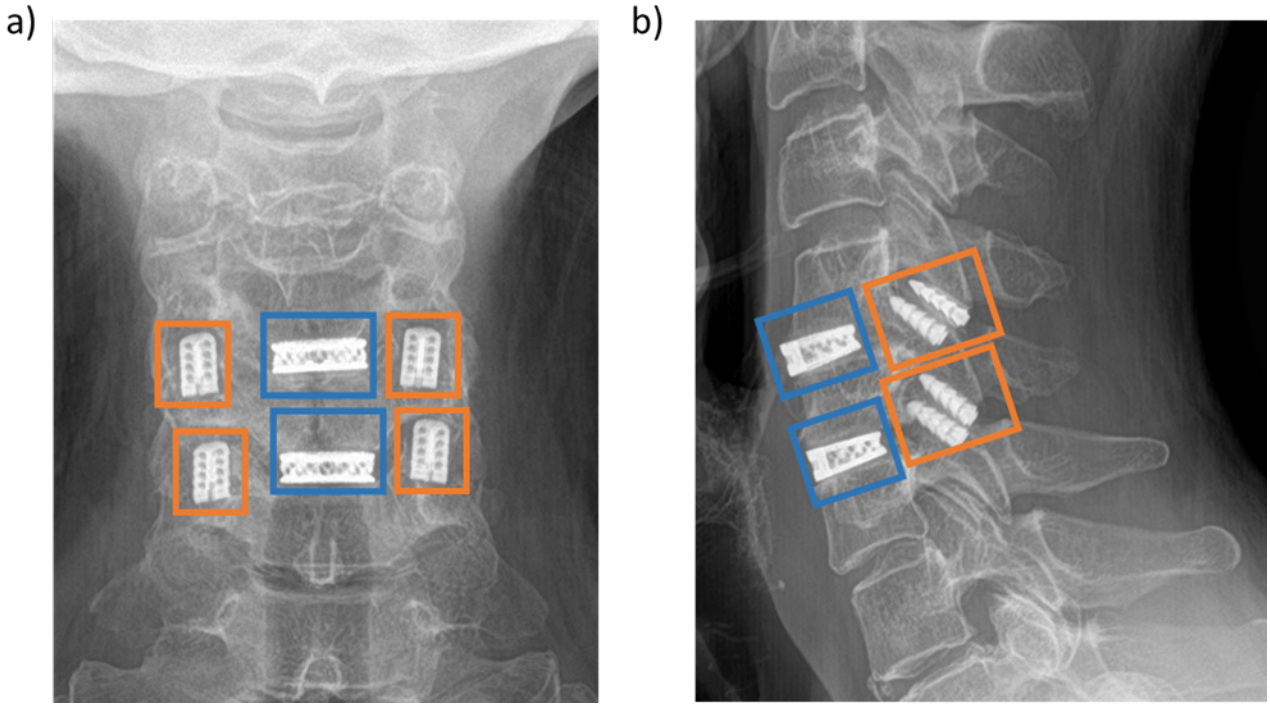


**Figure 2.** Posterior (a) and lateral (b) view of 60-year-old woman with the anterior disc cage (in blue) and the Sharkage (in orange).

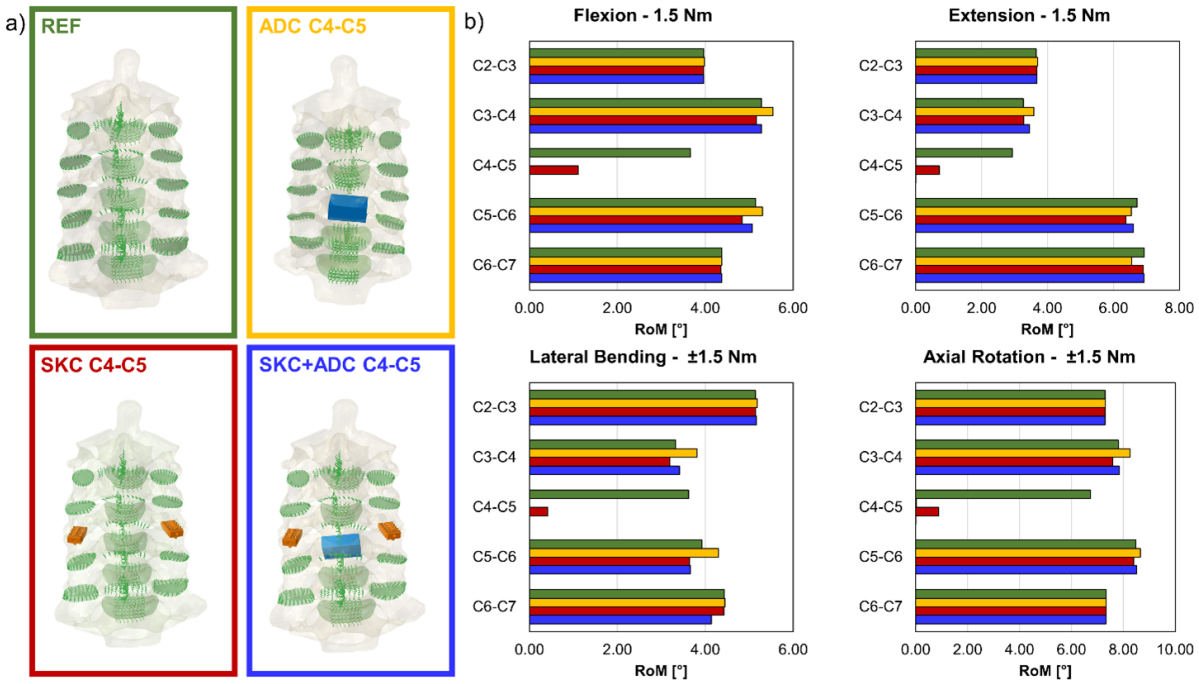


**Figure 3.** (a) The posterior view of REF, ADC, SKC, and SKC + ADC models with C4–C5 treated level. (b) Histograms of flexion, extension, lateral bending, and axial rotation (applying 1.5 Nm) for C2–C7 levels for all models. ADC, anterior disc cage; REF, reference; RoM, range of motion; SKC, Sharkage.

- SKC model: bilateral insertion of SKC devices between the posterior facets.
- SKC + ADC model: insertion of both the ADC and SKC devices, as described in the clinical case (Figure 2).

For each of the above simulations (I, II, and III), 3 different cases were evaluated to assess the influence of the treated level. Specifically, the C4–C5, C5–C6, and bilevel C4–C6 segments were analyzed (Figures 3A,

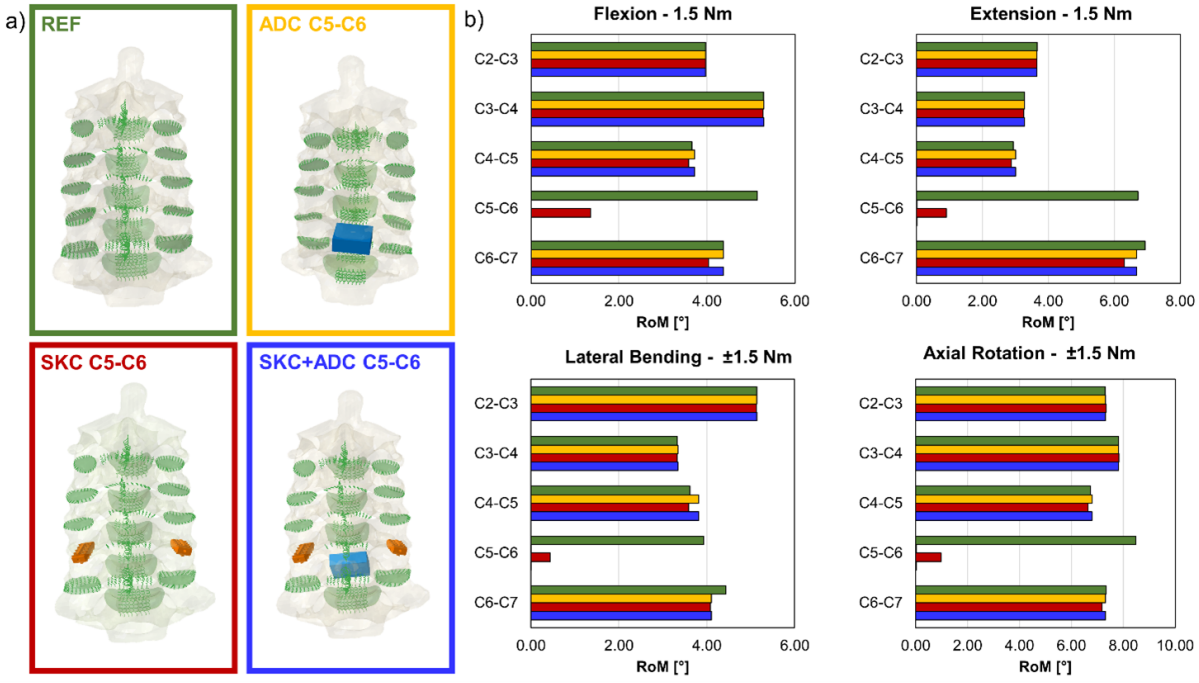


**Figure 4.** (a) The posterior view of REF, ADC, SKC, and SKC + ADC models with C5–C6 treated level. (b) Histograms of flexion, extension, lateral bending, and axial rotation (applying 1.5 Nm) for C2–C7 levels for all models. ADC, anterior disc cage; REF, reference; RoM, range of motion; SKC, Sharkage.

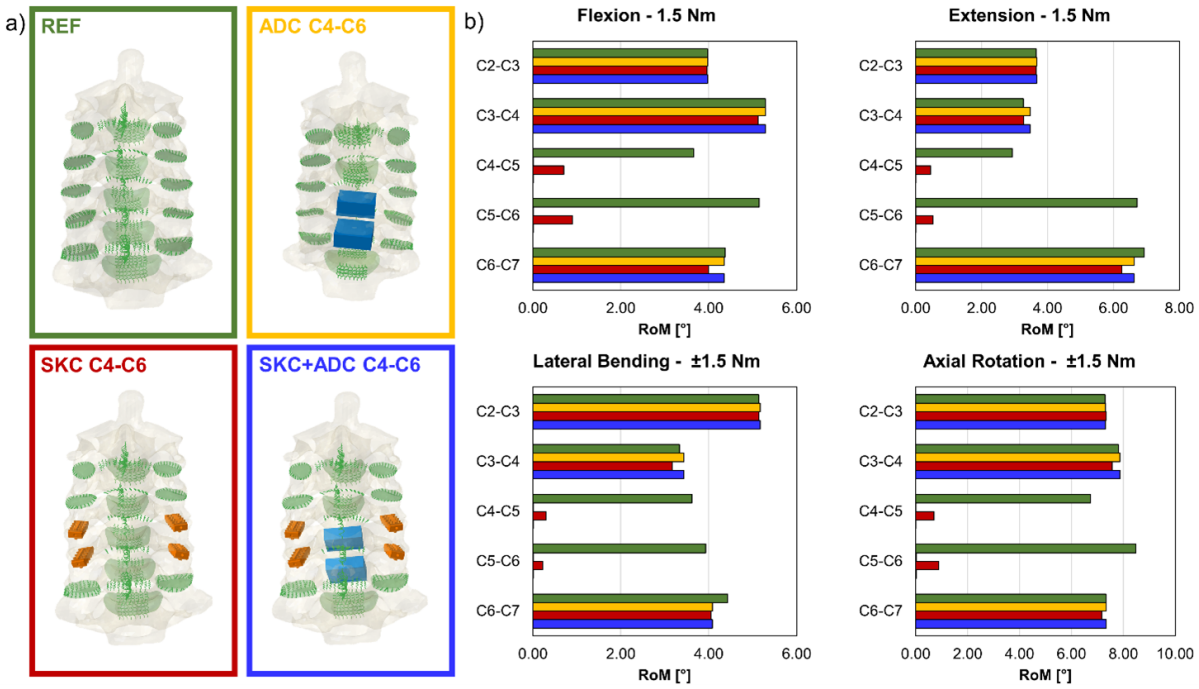


**Figure 5.** (a) The posterior view of REF, ADC, SKC, and SKC + ADC models with C4–C6 treated level. (b) Histograms of flexion, extension, lateral bending, and axial rotation (applying 1.5 Nm) for C2–C7 levels for all models. ADC, anterior disc cage; REF, reference; RoM, range of motion; SKC, Sharkage.

4A and 5A, respectively), the latter corresponding to the clinical case shown in Figure 2.

The SKC CAD model was provided by the manufacturer (2B1 s.r.l., Milan, Italy). A Ti6Al4V alloy linear-elastic material was assigned to the cage, with an elastic modulus (E) of 110 GPa and Poisson's ratio (ν) of 0.3. The SKC was positioned between the facets using an embedded region constraint, based on x-ray images, which simulates a fused bone-implant interface. The SKC model was meshed using 121,612 4-node linear tetrahedral elements (C3D4). At the treated level, the capsular ligament and facet cartilage were removed as required by the surgical procedure.

The ADC CAD was designed in Abaqus software as a solid trapezoid, deriving the dimensions from x-ray images (Figure 2). Young's modulus has been assigned considering a mean value between the solid (110 GPa) and trabecular (67 GPa) elastic modulus, weighted by the percentage of the respective occupied volume, resulting in a final modulus of 80 GPa.[36] After the excision of the intervertebral disc, anterior longitudinal ligament, and posterior longitudinal ligament, the ADC has been positioned into the empty cavity as depicted in the x-ray images, constrained to the vertebral column with an embedded region constraint and meshed with 70,864 4-node linear tetrahedrons (C3D4).

The interactions, boundary conditions, and loading conditions were consistent with the validated model as well as the material properties of the adjacent levels' discs. RoM and intradiscal pressure (IDP) were calculated and compared between models using values calculated for the validated model as a reference (REF). In addition, the percentage difference relative to the REF model in IDP values was calculated for each model and for each disc, where "NA" was reported in cases where a cage replaced the disc. Moreover, the RoM of the entire C2 to C7 spine segment was calculated and compared.

In addition, to investigate the biomechanics of the cervical spine of a patient who tends to replicate a physiologic motor task (compensating the constrained motion of the fixed segments with a muscular activation), a second hybrid-loading protocol was used in flexion.[37–39] In particular, a flexion moment was imposed to the model and able to obtain the same total RoM of the validated model when 1.5 Nm is applied, along with a preload of 50 N. The results of these further simulations (under the hybrid loading protocol) were evaluated. Outcomes of the hybrid loading protocol were the considering IDPs, which were then compared with those obtained when applying 1.5 Nm in flexion only.

## RESULTS

### Development and Validation of the C2–C7 Model

Figure 1 reports the intervertebral RoMs in flexion-extension, lateral bending, and axial rotation compared with the values derived from the literature (both

experimental and numerical data were considered), showing good agreement with the latter.

All RoMs were within 1 SD of either the numerical findings or the experimental data, except the C4–C5 segment in flexion-extension. Nevertheless, Herron et al[12] reported that the RoM of the C3–C7 segment of their model was 38.37°, and the C3–C7 RoM of the current model is 38.33°.

## Simulation of Different Clinical Scenarios

Results in terms of RoM of the ADC, SKC, and SKC + ADC models at the C4–C5, C5–C6, and C4–C6 treated levels are reported in Figures 3–5, respectively.

The use of ADC causes a complete elimination of the RoM at the treated level for all types of movement (flexion, extension, lateral bending, and axial rotation), together with an increase in the RoM in the adjacent segments. On the other hand, in the SKC model, the RoM at the levels where the SKC implant is placed is reduced by 75.6% (for C4–C5), 86.5% (for C5–C6), and 88.3% (average reduction for C4–C6 levels) compared with the REF model (the percentage reductions refer to extension but are similar for all movements). Furthermore, the RoM of the adjacent levels shows a decrease, contrary to what is observed with the ADC model.

Finally, the SKC + ADC model, similar to the ADC model, cancels the RoM at the level where the ADC device is present. However, for the adjacent segments, it shows an intermediate behavior between the SKC and ADC models. Specifically, there is a reduction in RoM compared with the REF model, although not as pronounced as in the SKC model (Figures 3b, 4b and 5b).

The percentage differences of IDPs of all models with respect to the REF model are reported in Table 2.

The SKC model, in which only the SKC is implanted, shows a mean IDP reduction of 69% in the treated level compared with all the other models. In addition, in the 2 adjacent levels, there is a reduction in IDP in all the cases, ranging from 1% to 7%, except in the scenario of extension with the implantation of SKC alone in C4 to C6, where IDP increases of 13%. Conversely, when ADC is used either alone or in combination with SKC, there is an increase in IDP at both the superior and inferior levels with respect to the treated one, ranging from 1% to 21%, particularly in the case of C4 to C6 extension with the SKC + ADC model.

Results in terms of total RoM of the validated model (REF) and the clinical models in flexion, extension, lateral bending, and axial rotation are reported in Table 3. As already observed in Figures 3–5, the SKC models show a

**Table 2.** Percentage reduction of intradiscal pressure (IDP) in each intervertebral disc for all models during flexion, extension, left and right bending, and left and right rotation, relative to the REF model.

| | | IDP in Flexion | | | | | IDP in Left Bending | | | | | IDP in Left Rotation | | | | |
|---|---|---|---|---|---|---|---|---|---|---|---|---|---|---|---|---|
| **Device** | | **d1** | **d2** | **d3** | **d4** | **d5** | **d1** | **d2** | **d3** | **d4** | **d5** | **d1** | **d2** | **d3** | **d4** | **d5** |
| Ref | $P_{max}$ (MPa) | 0.98 | 1.26 | 1.46 | 0.94 | 0.72 | 0.84 | 0.60 | 0.61 | 0.70 | 0.46 | 0.68 | 0.77 | 0.65 | 0.77 | 0.62 |
| C4–C5 | | | | | | | | | | | | | | | | |
| ADC | Reduction (%) | 0% | −2% | NA | −1% | 0% | −1% | −12% | NA | −3% | 0% | 0% | 2% | NA | 0% | 0% |
| SKC | | 0% | 1% | 45% | 3% | 0% | −1% | 1% | 70% | 2% | 0% | 0% | 2% | 58% | 1% | 0% |
| SKC + ADC | | 0% | 0% | NA | 1% | 0% | −1% | −4% | NA | 2% | 0% | 0% | 2% | NA | 0% | 0% |
| C5–C6 | | | | | | | | | | | | | | | | |
| ADC | Reduction (%) | 0% | 0% | −1% | NA | 0% | 1% | 1% | −3% | NA | 7% | −2% | −2% | −1% | NA | −1% |
| SKC | | 0% | 0% | 2% | 42% | 3% | 1% | 1% | −2% | 79% | 6% | −2% | −2% | −4% | 70% | 0% |
| SKC + ADC | | 0% | 0% | −3% | NA | −3% | 0% | 0% | −8% | NA | −2% | −2% | −2% | −1% | NA | −1% |
| C4–C6 | | | | | | | | | | | | | | | | |
| ADC | Reduction (%) | 0% | 0% | NA | NA | 0% | −1% | −3% | NA | NA | 8% | −2% | 1% | NA | NA | −1% |
| SKC | | 0% | 2% | 58% | 56% | 4% | 0% | 2% | 77% | 82% | 6% | −2% | 0% | 61% | 72% | 0% |
| SKC + ADC | | 0% | −2% | NA | NA | −3% | −1% | −12% | NA | NA | −2% | −1% | 0% | NA | NA | −1% |

| | | IDP in Extension | | | | | IDP in Right Bending | | | | | IDP in Right Rotation | | | | |
|---|---|---|---|---|---|---|---|---|---|---|---|---|---|---|---|---|
| | | **d1** | **d2** | **d3** | **d4** | **d5** | **d1** | **d2** | **d3** | **d4** | **d5** | **d1** | **d2** | **d3** | **d4** | **d5** |
| Ref | $P_{max}$ (MPa) | 0.57 | 0.48 | 0.81 | 0.78 | 0.75 | 0.84 | 0.64 | 0.71 | 0.49 | 0.56 | 0.75 | 0.83 | 0.81 | 0.77 | 0.47 |
| C4–C5 | | | | | | | | | | | | | | | | |
| ADC | Reduction (%) | −1% | −18% | NA | −5% | 0% | −1% | −6% | NA | −6% | 0% | 0% | 1% | NA | −1% | 0% |
| SKC | | 0% | 2% | 97% | 7% | 0% | 0% | 3% | 69% | 6% | 0% | 0% | 0% | 54% | 2% | 0% |
| SKC + ADC | | 0% | −5% | NA | 1% | 0% | −1% | 0% | NA | 5% | 0% | 0% | 2% | NA | −1% | 0% |
| C5–C6 | | | | | | | | | | | | | | | | |
| ADC | Reduction (%) | 0% | 0% | −2% | NA | 2% | −1% | −3% | −3% | NA | 2% | −1% | −1% | 0% | NA | −2% |
| SKC | | 0% | 1% | 2% | 105% | 7% | 0% | 7% | 13% | 69% | 23% | −1% | −1% | −1% | 65% | 0% |
| SKC + ADC | | 0% | −2% | −9% | NA | −5% | −1% | −1% | −8% | NA | −4% | −1% | −1% | 0% | NA | −2% |
| C4–C6 | | | | | | | | | | | | | | | | |
| ADC | Reduction (%) | −1% | −5% | NA | NA | 3% | −2% | −2% | NA | NA | 2% | −1% | 1% | NA | NA | −2% |
| SKC | | 3% | −13% | 71% | 83% | 2% | −1% | 3% | 76% | 68% | 2% | −1% | 0% | 63% | 71% | 0% |
| SKC + ADC | | −2% | −21% | NA | NA | −5% | −2% | −8% | NA | NA | −4% | −1% | 0% | NA | NA | −2% |

Abbreviations: ADC, anterior disc cage; NA, not available; Ref, reference; SKC, Sharkage.
*Note:* "d1" through "d5" indicate intervertebral discs. "d1" through "d5" indicate intervertebral discs. Postive numbers indicate a reduction in IDP, while negative numbers represents an increase in IDP. "NA" means that the ADC device is in place of the disc.

**Table 3.** Total RoM [°] under a 1.5 Nm load across different configurations in flexion, extension, lateral bending, and axial rotation.

| Measure | ADC | SKC | SKC + ADC |
|---|---|---|---|
| Flexion (Ref = 22.44°) | | | |
| C4–C5 | 19.22° | 19.43° | 18.70° |
| C5–C6 | 17.37° | 18.23° | 17.37° |
| C4–C6 | 13.62° | 14.71° | 13.62° |
| Extension (Ref = 23.52°) | | | |
| C4–C5 | 20.39° | 20.96° | 20.67° |
| C5–C6 | 16.62° | 17.00° | 16.62° |
| C4–C6 | 13.78° | 14.19° | 13.78° |
| Lateral Bending (Ref = 20.45°) | | | |
| C4–C5 | 17.76° | 16.83° | 16.38° |
| C5–C6 | 16.41° | 16.56° | 16.41° |
| C4–C6 | 12.70° | 12.92° | 12.70° |
| Axial Rotation (Ref = 37.64°) | | | |
| C4–C5 | 31.57° | 31.50° | 30.98° |
| C5–C6 | 29.29° | 29.95° | 29.29° |
| C4–C6 | 22.57° | 23.66° | 22.57° |

Abbreviations: ADC, anterior disc cage; Ref, reference; RoM, range of motion; SKC, Sharkage.

higher RoM with respect to ADC and SKC + ADC models in each movement and treated level, as expected.

With a constant applied angle of 22.44°, simulating the patient's compensatory mechanism to reproduce a pre-implant condition, in which the spine was able to achieve a greater rotation under a lower applied moment, IDPs were analyzed only during flexion. IDP values of all pathological models (SKC, ADC, and SKC + ADC) together with the percentage difference from those obtained with the application of a 1.5 Nm moment are reported in Table 4.

In each model, the tendency to replicate the physiological RoM leads to an increase in the IDPs that exceeds the IDPs of the REF model. Comparing the 3 clinical models (ADC, SKC, and SKC + ADC), the SKC models show less influence on the overloading of the discs in each treated level, confirming the trend in Table 2. In addition, given the higher mobility of the SKC models, the moment needed to reach the physiological motion is lower than that of the ADC and SKC + ADC models. Finally, the disc at the treated level in models SKC still experiences a decompression, though it is reduced if compared with the results of the models where a 1.5 Nm moment is applied.

# DISCUSSION

## Validation of the C2–C7 Model

In the present study, a C2–C7 FEM was developed, removing the cranium, C1, and the associated structures from the available model of Herron et al.[12] Since the implantation of the SKC, CIFS is not recommended at these levels according to the surgeon's indications. As already mentioned, the intervertebral RoMs of the model in flexion-extension, lateral bending, and axial rotation are in good agreement with experimental and numerical literature data; thus, the model could be considered validated. The validation did not take into account the IDPs of the model due to a lack of literature data regarding appropriate disc pressurization in flexion-extension, lateral bending, and axial rotation, as few studies include these data for the validated model or are incomplete or use different loading conditions with respect to the current model.

Subsequently, to explore the influence of the magnitude of preload and friction, 2 sensitivity analyses have been carried out. Focusing on the preload, the literature suggests

**Table 4.** IDP values at a physiological flexion angle of 22.44° (Table 3) across different clinical configurations.

| Device | Torque, Nm | | d1 | d2 | d3 | d4 | d5 |
|---|---|---|---|---|---|---|---|
| C4–C5 | | | | | | | |
| ADC | 1.75 | IDP (MPa) | 1.12 | 1.45 | NA | 1.08 | 0.82 |
| | | % diff | 14.2% | 12.4% | | 12.5% | 13.0% |
| SKC | 1.73 | IDP (MPa) | 1.10 | 1.39 | 0.89 | 1.01 | 0.81 |
| | | % diff | 13.1% | 11.3% | 11% | 10.7% | 12.0% |
| SKC + ADC | 1.80 | IDP (MPa) | 1.14 | 1.45 | NA | 1.07 | 0.84 |
| | | % diff | 17.1% | 14.6% | | 14.4% | 15.4% |
| C5–C6 | | | | | | | |
| ADC | 1.94 | IDP (MPa) | 1.22 | 1.53 | 1.85 | NA | 0.91 |
| | | % diff | 24.9% | 21.3% | 26.2% | | 25.7% |
| SKC | 1.85 | IDP (MPa) | 1.17 | 1.48 | 1.69 | 0.63 | 0.83 |
| | | % diff | 19.6% | 16.7% | 18.3% | 16.4% | 17.6% |
| SKC + ADC | 1.94 | IDP (MPa) | 1.22 | 1.53 | 1.81 | NA | 0.88 |
| | | % diff | 24.9% | 20.9% | 20.0% | | 19.1% |
| C4–C6 | | | | | | | |
| ADC | 2.47 | IDP (MPa) | 1.51 | 1.87 | NA | NA | 1.09 |
| | | % diff | 54.8% | 48.1% | | | 50.4% |
| SKC | 2.29 | IDP (MPa) | 1.41 | 1.70 | 0.85 | 0.56 | 0.95 |
| | | % diff | 44.4% | 36.6% | 37.2% | 35.7% | 36.8% |
| SKC + ADC | 2.47 | IDP (MPa) | 1.51 | 1.83 | NA | NA | 1.05 |
| | | % diff | 54.1% | 41.4% | | | 41.1% |

Abbreviations: ADC, anterior disc cage; IDP, intradiscal pressure; NA, not applicable; SKC, Sharkage.
*Note:* "NA" indicates ADC device is in place of the disc. The percentage difference is relative to the IDP obtained applying 1.5 Nm (see Table 2).

that its variation does not notably affect the results, and no significant difference is reported in the quality of the measured data.[17] The sensitivity analysis showed a variation in the RoM between the validated model (50 N) and those that use 0 and 100 N of preload that was not significant (lower than 9.5%), in accordance with the literature.[17] Moreover, a higher preload is associated with greater stability, which in turn is related to a reduction in RoM.[35] In fact, increasing the preload from 0 to 100 N leads to a reduction of the RoM, which could be associated with an enhancement of the stability.

Moving to the sensitivity analysis of the friction, results show that specifying a penalty of 0.1, instead of imposing a frictionless tangential behavior, does not lead to significantly different RoMs (the maximum variation is 5.2% in extension). However, a healthy synovial cartilage has a friction coefficient that is below 0.05; therefore, its modeling with a penalty of 0.1 is not representative of its physiological behavior.[40]

## Simulation of Different Clinical Scenarios

The validated model (REF) was successfully used to analyze various clinical scenarios inspired by a representative case of a 60-year-old woman with right cervical radiculopathy caused by an osteophytic discopathy with foraminal stenosis at C4-C5-C6, who underwent surgery to implant 2 SKC and 2 ADCs at levels C4–C6 (Figure 2). Based on this case, 3 different models were developed to compare 3 different surgical techniques: ADC alone, SKC alone, and a combination of the 2 (SKC + ADC). In addition, 3 conditions were simulated for each model to assess the influence of treatment at different levels (C4–C5, C5–C6, and C4–C6).

In general, the use of SKC significantly reduces the RoM, up to a maximum of 94% in axial rotation in the C4–C6 model. However, it does not completely eliminate the RoM at the treated level, which may lead to an increased risk of pseudarthrosis; on the contrary, with ADC, the RoM was eliminated where the device is implanted, resulting in greater spinal stability. The increased mobility allowed by SKC is further confirmed by analyzing the total RoM over different simulated movements. As shown in Table 3, the RoM in the SKC model reduces by a maximum of 59% in axial rotation at C4 to C6, compared with a 67% reduction with ADC. The increased mobility with SKC primarily results in a reduced load on the disc, leading to an overall reduction in IDPs at all levels. At the treated level, SKC produces a maximum IDP decrease of approximately 105% (the maximum value was obtained in extension with C5–C6 treated).

When analyzing the levels adjacent to the treated one, SKC leads to a slight reduction in mobility in the adjacent segments (up to 10.5% in right bending when C4–C6 are treated), unlike the ADC model, where hypermobility is observed (Figures 3–5). When both SKC and ADC are used in combination, slight hypermobility is maintained regardless of the involved level.

As expected, in adjacent levels with SKC, the IDP generally decreases, resulting in decompression or shielding of the disc. In contrast, the hypermobility induced by ADC (both ADC and SKC + ADC models) leads to an increased IDP, which may indicate overloading and affect nutrient exchange, potentially increasing the probability of postoperative disc degeneration.[5] In addition, it may result in a higher potential of pseudarthrosis.[5]

The analysis of the total RoM shows that, as mentioned above, the SKC model allows the cervical spine to have global mobility that is closer to the physiological one; therefore, the treated level is less stiff than that of ADC and SKC + ADC models. This may be beneficial if the patient compensates with muscular activation for losing RoM. When the global physiological RoM is restored, specifically by imposing 22.44° in flexion as in this study, IDPs increase in all models (ADC, SKC, and SKC + ADC). However, the SKC stand-alone model requires a lower moment (indicating less muscular effort) and shows a smaller increase in IDP compared with the ADC and SKC + ADC models, as shown in Table 4.

As in the previous analysis, where a bending moment of 1.5 Nm was applied, imposing an angle equivalent to the physiological one results in lower IDPs for the SKC model compared with the ADC and SKC + ADC cases, confirming the trend.

A notable difference between the 2 analyses is that when the same angle is applied, IDPs increase in all cases except in the discs at the surgical level (SKC model). On the other hand, when the torque is applied, both increases and decreases in IDPs are observed, particularly a reduction in the levels adjacent to the treated ones, as shown in Table 3.

Furthermore, considering the variations observed between the treated levels (C4–C5 vs C5–C6 vs C4–C6), the C4–C6 segment is the stiffest under both loading conditions: (i) an applied torque of 1.5 Nm and (ii) an imposed flexion angle of 22.44°. Specifically, in condition (i), the reduction in RoM at the treated levels is more pronounced for C4–C6 compared with single-level treatments. In condition (ii), the C4–C6 case in the ADC and SKC + ADC models requires a maximum torque of 2.47 Nm to achieve the same RoM as the REF model, indicating how much the muscles must compensate to impose a flexion

equivalent to that of a condition without implanted devices (22.44° of flexion), resulting in a greater increase in IDPs at the adjacent levels (Table 4). These findings align with the established literature, which consistently reports that when motion at the operated or fused segment is restricted, adjacent levels compensate by increasing their RoM. This compensatory hypermobility leads to higher IDPs and is considered a contributing factor to adjacent-segment degeneration.[5,14,17,18,37,39,41,42] In this context, the results confirm that muscular and neural compensation attempts to restore preimplant motion, thereby increasing the loads and IDPs at both the treated and adjacent segments.

### Limitations

Some limitations must be acknowledged. First, in the models simulating the clinical cases, pathology was not explicitly modeled, and the spine was assumed to have the curvatures of a healthy individual after implantation of the different cages. In addition, muscles and their effects were excluded from this study. Second, as described above, an embedded interaction was used between the device and the bone to simplify the device-bone interaction. This approach prevents any movement between the 2 components, simulating the device as fully osseointegrated. This could overestimate the SKC stability and ignore the early postoperative phase when micromovements could occur, potentially leading to cage displacement under excessive loading (worst case scenario). Finally, regarding the geometries of the implanted devices, the SKC 3D model was provided by the manufacturer, while, for the ADC model, a simplified trapezoidal shape was used with material properties adjusted to account for its trabeculated structure, resulting in a lower overall modulus (80 GPa) compared with standard titanium alloy (110 GPa).[36]

Finally, the study highlights that CIFS alone could represent a cost-effective, less invasive, and equally effective alternative to combined CIFS and ADC fusion for selected patients, offering sufficient spinal stabilization while reducing surgical time. However, careful patient selection and postoperative rehabilitation are crucial to mitigate the risks of pseudarthrosis, adjacent segment degeneration, and excessive muscular compensation.[5,38]

## CONCLUSION

In conclusion, this study focused on developing and validating a FEM of the C2–C7 cervical spine, which was then used to investigate a specific clinical scenario. The primary goal was to determine whether the SKC, a CIFS designed by 2B1 S.r.l., implanted as a stand-alone solution, was comparable to an ADC implant or to the combination of the 2 systems (SKC + ADC). Remarkably, in several cases, the stand-alone SKC implant resulted in a greater RoM of the cervical spine while reducing IDP. This suggests that the stand-alone SKC system may offer significant benefits to patients, both mechanically and clinically.

## ACKNOWLEDGMENTS

The authors gratefully acknowledge Carlo Miglietta (2B1 s.r.l., Milan, Italy) for his support of the study and for supplying the CAD models necessary for the numerical analysis.

## REFERENCES

1. Masson de Almeida Prado R, Masson de Almeida Prado JL, Ueta RHS, Guimarães JB, Yamada AF. Subaxial spine trauma: radiological approach and practical implications. *Clin Radiol*. 2021;76(12):941. doi:10.1016/j.crad.2021.09.006

2. Podlewski S, Kłębczyk A, Radek M. Degenerative cervical spine disease: pathogenesis and symptoms. *Med Stud Med*. 2020;36(4):310–315. doi:10.5114/ms.2020.102326

3. Kushchayev SV, Glushko T, Jarraya M, et al. ABCs of the degenerative spine. *Insights Imaging*. 2018;9(2):253–274. doi:10.1007/s13244-017-0584-z

4. *Spondylosis*. Yale Medicine. https://www.yalemedicine.org/conditions/spondylosis.

5. Hua W, Zhi J, Ke W, et al. Adjacent segment biomechanical changes after one- or two-level anterior cervical discectomy and fusion using either a zero-profile device or cage plus plate: a finite element analysis. *Comput Biol Med*. 2020;120:103760. doi:10.1016/j.compbiomed.2020.103760

6. de Jager M. *Mathematical Modelling of the Human Cervical Spine*. Eindhoven, The Netherlands: Technische Universiteit Eindhoven; 1993:213–227.

7. Leasure JM, Buckley J. Biomechanical evaluation of an interfacet joint decompression and stabilization system. *J Biomech Eng*. 2014;136(7):0710101–0710108. doi:10.1115/1.4026363

8. Tan LA, Straus DC, Traynelis VC. Cervical interfacet spacers and maintenance of cervical lordosis. *J Neurosurg Spine*. 2015;22(5):466–469. doi:10.3171/2014.10.SPINE14192

9. Kasliwal MK, Corley JA, Traynelis VC. Posterior cervical fusion using cervical interfacet spacers in patients with symptomatic cervical pseudarthrosis. *Neurosurgery*. 2016;78(5):661–668. doi:10.1227/NEU.0000000000001087

10. Cofano F, Sciarrone GJ, Pecoraro MF, et al. Cervical interfacet spacers to promote indirect decompression and enhance fusion in degenerative spine: a review. *World Neurosurg*. 2019;126:447–452. doi:10.1016/j.wneu.2019.03.114

11. Hah RJ, Alluri R, Anderson PA. Biomechanical analysis of an anterior cervical discectomy and fusion pseudarthrosis model revised with machined interfacet allograft spacers. *Global Spine J*. 2020;10(8):973–981. doi:10.1177/2192568219884265

12. Herron MR, Park J, Dailey AT, Brockmeyer DL, Ellis BJ. Febio finite element models of the human cervical spine. *J Biomech*. 2020;113:110077. doi:10.1016/j.jbiomech.2020.110077

13. Duan Y, Zhang H, Min SX, Zhang L, Jin AM. Posterior cervical fixation following laminectomy: a stress analysis of three techniques. *Eur Spine J*. 2011;20(9):1552–1559. doi:10.1007/s00586-011-1711-z

14. Huang W, Tian Y, Wang H, et al. Comparative analysis of the biomechanics of anterior cervical discectomy and fusion with multiple segmental plates fixation versus single multilevel plate fixation: a finite element study. *BMC Musculoskelet Disord*. 2022;23(1):848. doi:10.1186/s12891-022-05796-7

15. Lin M, Paul R, Dhar UK, et al. A review of finite element modeling for anterior cervical discectomy and fusion. *Asian Spine J*. 2023;17(5):949–963. doi:10.31616/asj.2022.0295

16. Silva AJC, de Sousa RJA, Fernandes FAO, Ptak M, Parente MPL. Development of a finite element model of the cervical spine and validation of a functional spinal unit. *SSRN Journal*. 2022. doi:10.2139/ssrn.4177758

17. Mo ZJ, Zhao YB, Wang LZ, Sun Y, Zhang M, Fan YB. Biomechanical effects of cervical arthroplasty with U-shaped disc implant on segmental range of motion and loading of surrounding soft tissue. *Eur Spine J*. 2014;23(3):613–621. doi:10.1007/s00586-013-3070-4

18. Wo J, Lv Z, Wang J, et al. Biomechanical analysis of cervical artificial disc replacement using cervical subtotal discectomy prosthesis. *Front Bioeng Biotechnol*. 2021;9:680769. doi:10.3389/fbioe.2021.680769

19. Devin Leahy P. *Assessment of the Effects of Ligamentous Injury in the Human Cervical Spine*. Fort Collins, Colorado, USA: Colorado State University; 2012. doi:10.1016/j.jbiomech.2012.08.012

20. Panzer MB, Fice JB, Cronin DS. Cervical spine response in frontal crash. *Med Eng Phys*. 2011;33(9):1147–1159. doi:10.1016/j.medengphy.2011.05.004

21. Erbulut DU, Zafarparandeh I, Lazoglu I, Ozer AF. Application of an asymmetric finite element model of the C2-T1 cervical spine for evaluating the role of soft tissues in stability. *Med Eng Phys*. 2014;36(7):915–921. doi:10.1016/j.medengphy.2014.02.020

22. Wheeldon JA, Stemper BD, Yoganandan N, Pintar FA. Validation of a finite element model of the young normal lower cervical spine. *Ann Biomed Eng*. 2008;36(9):1458–1469. doi:10.1007/s10439-008-9534-8

23. Rahman WU, Jiang W, Wang G, Li Z. Numerical investigation on the stability of human upper cervical spine (C1–C3). *Biomed Mater Eng*. 2022;33(3):169–181. doi:10.3233/BME-211247

24. Lee S-H, Im Y-J, Kim K-T, Kim Y-H, Park W-M, Kim K. Comparison of cervical spine biomechanics after fixed- and mobile-core artificial disc replacement. *Spine (Phila Pa 1986)*. 2011;36(9):700–708. doi:10.1097/BRS.0b013e3181f5cb87

25. Östh J, Brolin K, Svensson MY, Linder A. A female ligamentous cervical spine finite element model validated for physiological loads. *J Biomech Eng*. 2016;138(6). doi:10.1115/1.4032966

26. Lin D, He Z, Weng R, et al. Comparison of biomechanical parameters of two chinese cervical spine rotation manipulations based on motion capture and finite element analysis. *Front Bioeng Biotechnol*. 2023;11:1–12. doi:10.3389/fbioe.2023.1195583

27. Mustafy T, El-Rich M, Mesfar W, Moglo K. Investigation of impact loading rate effects on the ligamentous cervical spinal load-partitioning using finite element model of functional spinal unit C2-C3. *J Biomech*. 2014;47(12):2891–2903. doi:10.1016/j.jbiomech.2014.07.016

28. White AA, Panjabi MM. *Clinical Biomechanics of the Spine*. 2nd ed. Park Avenue, New York, USA: Lippincott; 1990.

29. Lysell E. Motion in the cervical spine. An experimental study on autopsy specimens. *Acta Orthop Scand*. 1969:6470. doi:10.3109/ort.1969.40.suppl-123.01

30. Wheeldon JA, Pintar FA, Knowles S, Yoganandan N. Experimental flexion/extension data corridors for validation of finite element models of the young, normal cervical spine. *J Biomech*. 2006;39(2):375–380. doi:10.1016/j.jbiomech.2004.11.014

31. Nightingale RW, Winkelstein BA, Knaub KE, Richardson WJ, Luck JF, Myers BS. Comparative strengths and structural properties of the upper and lower cervical spine in flexion and extension. *J Biomech*. 2002;35(6):725–732. doi:10.1016/s0021-9290(02)00037-4

32. Nightingale RW, Carol Chancey V, Ottaviano D, et al. Flexion and extension structural properties and strengths for male cervical spine segments. *J Biomech*. 2007;40(3):535–542. doi:10.1016/j.jbiomech.2006.02.015

33. Finn MA, Brodke DS, Daubs M, Patel A, Bachus KN. Local and global subaxial cervical spine biomechanics after single-level fusion or cervical arthroplasty. *Eur Spine J*. 2009;18(10):1520–1527. doi:10.1007/s00586-009-1085-7

34. Camacho DL, Nightingale RW, Robinette JJ, Vanguri SK, Douglas J, Coates BSM. Experimental flexibility measurements for the development of a computational head-neck model validated for near-vertex head impact. *SAE Tech Pap*. 1997;14:973345. doi:10.4271/973345

35. Huang S, Ling Q, Lin X, Qin H, Luo X, Huang W. Biomechanical evaluation of a novel anterior transpedicular screw-plate system for anterior cervical corpectomy and fusion (ACCF): a finite element analysis. *Front Bioeng Biotechnol*. 2023;11:1–11. doi:10.3389/fbioe.2023.1260204

36. Danielli F, Ciriello L, La Barbera L, Rodriguez Matas JF, Pennati G. On the need of a scale-dependent material characterization to describe the mechanical behavior of 3D printed ti6al4v custom prostheses using finite element models. *J Mech Behav Biomed Mater*. 2023;140:105707. doi:10.1016/j.jmbbm.2023.105707

37. Purushothaman Y, Yoganandan N, Jebaseelan D, Choi H, Baisden J. External and internal responses of cervical disc arthroplasty and anterior cervical discectomy and fusion: a finite element modeling study. *J Mech Behav Biomed Mater*. 2020;106:103735. doi:10.1016/j.jmbbm.2020.103735

38. Tan LA, Yoganandan N, Choi H, Purushothaman Y, Jebaseelan D, Bosco A. Biomechanical analysis of 3-level anterior cervical discectomy and fusion under physiologic loads using a finite element model. *Neurospine*. 2022;19(2):385–392. doi:10.14245/ns.2143230.615

39. Ouyang P, Li J, He X, et al. Biomechanical comparison of 1-level corpectomy and 2-level discectomy for cervical spondylotic myelopathy: a finite element analysis. *Med Sci Monit*. 2020;26:e919270. doi:10.12659/MSM.919270

40. Mengoni M. Biomechanical modelling of the facet joints: a review of methods and validation processes in finite element analysis. *Biomech Model Mechanobiol*. 2021;20(2):389–401. doi:10.1007/s10237-020-01403-7

41. Eck JC, Humphreys SC, Lim T-H, et al. Biomechanical study on the effect of cervical spine fusion on adjacent-level intradiscal pressure and segmental motion. *Spine (Phila Pa 1976)*. 2002;27(22):2431–2434. doi:10.1097/00007632-200211150-00003

42. Hua W, Zhi J, Wang B, et al. Biomechanical evaluation of adjacent segment degeneration after one- or two-level anterior cervical discectomy and fusion versus cervical disc arthroplasty:

a finite element analysis. *Comput Methods Programs Biomed*. 2020;189:105352. doi:10.1016/j.cmpb.2020.105352

**Funding:** The authors received no financial support for the research, authorship, and/or publication of this article.

**Declaration of Conflicting Interests:** The authors report no conflicts of interest in this work.

**Author Contributions:** Luca Ciriello: conceptualization, data curation, formal analysis, funding acquisition, investigation, methodology, software, validation, visualization, and roles/writing—original draft. Margherita Rotondi: data curation, formal analysis, funding acquisition, investigation, methodology, software, validation, visualization, and roles/writing—original draft. Giuseppe Sciarrone: conceptualization, formal analysis, investigation, resources, supervision, roles/writing—original draft, and writing—review and editing. Tomaso Villa: conceptualization, data curation, formal analysis, investigation, methodology, project administration, resources, supervision, validation, visualization, roles/writing—original draft, and writing—review and editing.

**Corresponding Author:** Tomaso Villa, Department of Chemistry, Materials and Chemical Engineering "Giulio Natta" - LaBS, Politecnico di Milano, Piazza L. da Vinci 32, Milan, Italy; tomaso.villa@polimi.it

Published 10 March 2026